Journal of Alloys and Compounds 509 (2011) 6871–6875

Contents lists available at ScienceDirect

Journal of Alloys and Compounds

journal homepage: www.elsevier.com/locate/jallcom

Effect of oxidation at 1100 °C on the strength of ZrB_2–SiC–graphite ceramics

Wang Zhi [a], Qu Qiang [b], Wu Zhanjun [a,*], Shi Guodong [a]

[a] School of Aeronautics and Astronautics, Faculty of Vehicle Engineering and Mechanics, State Key Laboratory of Structural Analysis for Industrial Equipment, Dalian University of Technology, Dalian 116024, China
[b] China Academy of Launch Vehicle Technology R&D Centre, Beijing 100076, China

ARTICLE INFO

Article history:
Received 23 December 2010
Received in revised form 28 March 2011
Accepted 29 March 2011
Available online 5 April 2011

Keywords:
Zirconium diboride
Surface oxidation
Microstructure

ABSTRACT

One standard surface crack was introduced at the center of the tension surface of the test specimens with a Vickers indenter to investigate the effect of oxidation on the strength of ZrB_2–SiC–graphite ceramic. The flexural strength of the pre-cracked specimen was 371.7 MPa, which was lower than the strength of ~500 MPa for the original ceramic. Oxidation in dry or moist air was employed for 30, 60, or 90 min. The flexural strength of the oxidized specimens increased as the oxidation time increased up to 60 min and then the flexural strength did not further increase. The flexural strength of specimens oxidized in dry air was greater than those specimens oxidized in moist air, which revealed that the compounds of glassy structure could better heal the cracks on the surface of the specimen than the compounds of lamellar structure. The strength of the oxidized specimen was comparable to the strength of the pre-cracked specimens.

1. Introduction

Zirconium diboride (ZrB_2) is a potential candidate for a variety of high temperature structural applications, such as furnace elements [1], plasma arc electrodes [2], hypersonic aircraft [3], reusable launch vehicles [4], or rocket engines and thermal protection structures for leading edge parts on hypersonic reentry space vehicles [5]. Because of recent efforts to develop hypersonic aerospace vehicles and re-usable atmospheric re-entry vehicles, interest in UHTCs has significantly increased in the past few years. As a result, groups in the United States, Italy, Japan, India, and China are investigating ZrB_2-based ceramics [6]. Until now, it is known that the addition of appropriate amounts of SiC particles not only enhances the mechanical properties, but also improves the oxidation resistance of ZrB_2 by promoting the formation of silicate-based glasses that inhibit oxidation at temperatures between 800 and 1700 °C [7]. However, unsatisfactory fracture toughness is still obstacle for them to be used widely, especially for applications in severe environments [8]. Our previous works have confirmed that the fracture toughness as low as 4.5 MPa $m^{1/2}$ of the ZrB_2–SiC composites was further improved to 6.1 MPa $m^{1/2}$ by adding the graphite flake [9]. The cracks on the surface of the polished specimen were found as a result of the significant pullout or desquamation of the graphite flake during the process of polishing surface because of weak bonding caused by the presence of the graphite flake within the ZrB_2–SiC–graphite ceramic. These surface slots or pits in the ZrB_2–SiC–graphite ceramic are indeed due to graphite flake pullout and/or desquamation and not due to incomplete densification [9]. Generally speaking, ZrB_2 based ceramics are brittle and sensitive to cracks. As a result, the structural integrity of the ZrB_2–SiC–graphite ceramic components may be seriously affected. In order to overcome this disadvantage, there are two ways: (a) inspect carefully and repair the unacceptable cracks, (b) heal the cracks and recover strength [11,12]. For method (a), allowable cracks in ceramics are so small that it is almost impossible to detect the cracks. Moreover, structural ceramics are so brittle that repair is almost impossible. For method (b), very few studies have been made of method (b). Some ceramics containing silicon and/or aluminum element have the ability to heal a cracks, which is in favor of increases in the reliability of structural ceramic components [12]. When the ZrB_2–SiC–graphite ceramic is exposed to high temperature air, the surface of the ZrB_2–SiC–graphite ceramic begins to oxidize to oxides. For instance, ZrB_2 is oxidized to ZrO_2 and B_2O_3 above 650 °C [13]; SiC is oxidized to SiO_2 above 900 °C [14]; Graphite flake is oxidized to CO above 500 °C [15]. So, SiO_2 and B_2O_3 glasses could be formed at high temperature. Furthermore, the SiO_2 can react with B_2O_3 to form a borosilicate glass [16].

Crack healing behavior is very sensitive to crack-healing conditions, such as crack healing temperature and time as well as atmosphere. Therefore, in this paper, the effect of the crack-healing conditions on flexural strength of a ZrB_2–SiC–graphite ceramic was investigated in detail. The surface microstructure of a ZrB_2–SiC–graphite ceramic after oxidation at 1100 °C in air was also investigated.

* Corresponding author. Tel.: +86 411 84706791; fax: +86 411 84706791.
E-mail address: wzdlut@dlut.edu.cn (W. Zhanjun).

0925-8388/$ – see front matter © 2011 Elsevier B.V. All rights reserved.
doi:10.1016/j.jallcom.2011.03.163

2. Experimental

Commercially available ZrB_2 powder (2 μm, >99.5%, Northwest Institute for nonferrous metal research, China), SiC (1 μm, >99.5%, Weifang Kaihua Micro-powder Co., Ltd., China.) and the graphite flake (mean diameter and thickness are 15 μm and 1.5 μm, respectively, >99%, Qingdao Tiansheng graphite Co., Ltd., China) were used as raw powders. The powder mixture of ZrB_2 plus 20 vol.% SiC plus 15 vol.% graphite flake was mixed using a planetary mill (Nanjing University planetary mill Co., Ltd., China) at 260 rotations per minute for 10 h in a polyethylene bottle using ZrO_2 balls and ethanol as the grinding media. After mixing, the slurry was dried in a rotary evaporator and screened by sizing screen with 800 meshes. Then the mixture was hot-pressed at 1900 °C for 1 h under a uniaxial load of 30 MPa in Ar atmosphere. The flexural strength of the specimens before and after heat treatment was tested in three point bending on 3 mm × 4 mm × 36 mm bars, using a 30 mm span and a crosshead speed of 0.5 mm min^{-1}. Prior to treatment, each specimen was ground and polished with diamond slurries down to a 1 μm finish, and the edges of all the specimens were chamfered to minimize the effect of stress concentration due to machining cracks. A minimum number of five specimens were tested for each condition. One standard surface crack was introduced at the center of the tension surface of the test specimens with a Vickers indenter using a load of 49 N for 15 s. The polished rectangular bars were heated at the temperature of 1100 °C for certain time, then slowly cooled to room temperature. The heating and cooling rates were 30 °C min^{-1} and 10 °C min^{-1}, respectively. Two healing environments were adopted: dry air and saturated moist air, healing time for each condition is 30, 60 and 90 min, respectively. The absolute dry air and water vapor was mixed and the relative humidities of the dry and moist air at room temperature were conditioned to 0.4% and 35%, respectively. The mixed air was pumped into the reaction chamber. After oxidation, the specimens were kept in a sealed container, which was protected from ambient moisture to prevent hydration of B_2O_3. The microstructural observations of specimen were carried out by scanning electron microscopy (SEM, FEI Sirion, Holland) along with energy dispersive spectroscopy (EDS, EDAX Inc) for chemical analysis. For the crystalline phase analysis, grazing incidence X-ray diffraction (GXRD; X'Pert MRD, Panalytical, Almelo, Netherlands) was used to determine the crystalline phases of coatings. The incidence angle for GXRD was set to 1°, which resulted in a penetration depth of less than 200 nm into the specimen.

3. Results and discussion

3.1. Microstructure

SEM images of the surface shapes and cross-sectional shapes of the crack and indentation are presented in Fig. 1. EDS and XRD analysis confirmed (not shown here) that the small darker phase was SiC and it dispersed uniformly in the lighter ZrB_2 matrix, the long and narrow darker phase and the slots in the surface of the specimen were graphite. The ZrB_2–SiC–graphite ceramic showed evidence of graphite desquamation (slots) during polishing because of weak interface bonding caused by the presence of graphite in the ZrB_2–SiC–graphite ceramic [10]. It was evident from the high relative density of 99.6% that these surface pits in the ZrB_2–SiC–graphite ceramic were indeed due to graphite flake desquamation and not due to incomplete densification. As a result, the slots in the surface of specimen were detrimental to the mechanical properties and the structural integrity of the ZrB_2–SiC–graphite ceramic because ZrB_2 based ceramics are brittle and sensitive to cracks on the surface of the measured specimen. The Griffith fracture criterion was applied based on the brittle fracture behavior of the ZrB_2–SiC–graphite ceramic. For sharp cracks which result in a $\alpha^{-1/2}$ singular stress field, the ZrB_2–SiC–graphite ceramic failure can be characterized by the Griffith fracture criterion based on fracture mechanics theory in terms of half crack length, α_{cr}:

$$a_{cr} \approx \frac{{K_{IC}}^2}{\sigma^2 \pi} \quad (1)$$

where α_{cr} is critical crack size for brittle fracture. σ, is the critical stress which will cause propagation of a crack-like flaw, α_{cr}. K_{IC}, is a material property referred to the fracture toughness. That is to say, the Griffith fracture criterion describes the critical flaw size that can occur without catastrophic crack propagation for brittle materials. The critical flaw size was calculated to 47.8 μm based on the fracture toughness of 6.11 MPa m$^{1/2}$ and flexural strength of 498.8 MPa for the ZrB_2–SiC–graphite [7,8]. The typical crack propagation paths are inserted in Fig. 1A. The radial crack at the edge of Vickers' indentation clearly revealed that the crack propagation path was altered by the addition of graphite flake by crack deflection, branching and crack bridging. The deformation induced by stress using Vickers' indentation was readily observed in the cross-section as shown in Fig. 1B.

The surface of the ZrB_2–SiC–graphite ceramic was oxidized to oxides at 1100 °C. These main reactions during the oxidation process were expected as follows:

$$2C(s) + O_2 \rightarrow 2CO(g) \quad (2)$$

$$ZrB_2(s) + 5/2O_2 \rightarrow ZrO_2(s) + B_2O_3 \quad (3)$$

$$2SiC(s) + 3O_2 \rightarrow 2SiO_2(l) + 2CO(g) \quad (4)$$

$$xSiO_2(l) + yB_2O_3(l) \rightarrow xSiO_2{\cdot}yB_2O_3 \quad (5)$$

The micrograph of the surface of the specimen oxidized for 30 min in dry air is shown in Fig. 2A. The Vickers' indentation on the surface of the specimen after oxidation was not found due to the formation of the oxide layers. The compounds of glassy structure were readily observed on the surface of the specimen. The EDS analysis confirmed that glass layer mainly composed of oxygen element and a small quantity of Si and Zr elements, which was consistent with the presence of B_2O_3 [14]. This may be due to the oxidation time limited the oxidation of SiC, indicating that 30 min was not enough for SiO_2 formation at 1100 °C under stagnant air because the oxidation of SiC is much slower than that of ZrB_2 in this temperature regime, the SiC particles could not be obviously oxidized. The B_2O_3 layer is expected to contain a small quantity of SiO_2 during long heating at 1100 °C based on the slight oxidation of the SiC by reactions (4) and (5). Moreover, ZrO_2 grains could not be detected due to a B_2O_3-rich layer was found to form above the ZrO_2 layer because of volume expansion upon conversion of ZrB_2 to ZrO_2 and B_2O_3 (~300% volume expansion based on density calculations) and/or the mutual wetting behavior of the two materials [14]. The slots resulted from oxidation of the graphite flake were easily observed below a B_2O_3-rich glass, which revealed that the slots on the surface of the specimen were not healed by a B_2O_3-rich glass in 30 min due to the rapid volatilization of a B_2O_3-rich glass because the B_2O_3-rich glass with low viscosity had a higher vapor pressure [13]. In addition, the escape of CO resulted from oxidation of the graphite flake led to that liquid B_2O_3 is difficult to spread to the defect.

Fig. 2B shows the micrograph of the surface of the specimen oxidized for 60 min in dry air. The EDS analysis confirmed that the glass layer was composed of oxygen with small quantities of Si and Zr, which was consistent with the presence of a B_2O_3-rich glass. As the oxidation time increased and B_2O_3 volatilized, the amount of SiC oxidation increased, which resulted in the formation of a borosilicate glass. The Zr was detected in the glass layer because of the thinner glass layer that formed due to the volatilization of B_2O_3 at 1100 °C [13]. The presence of crossed-cracks in the glass layer was presumably ascribed to volume shrinkage during cooling. The micrograph of the surface of the specimen oxidized for 90 min in dry air was similar to that of the specimen oxidized for 60 min in dry air.

Fig. 3A shows the micrograph of the surface of the specimen oxidized for 30 min in moist air. The surface of the specimen was covered with the lamellar particles and a small quantity of the glass phase which was borosilicate glass and/or unreacted B_2O_3 glass. As treatment time increased, the surface of the specimen did not change compared with the surface of the specimen oxidized for 30 min in moist air. The typical GXRD spectrum obtained from the surface of the specimen oxidized for 60 min in moist air is shown in Fig. 3B. Apparently, the phase analysis indicated the predominant phases for the oxidized specimen were ZrO_2, H_3BO_3 and a trace of

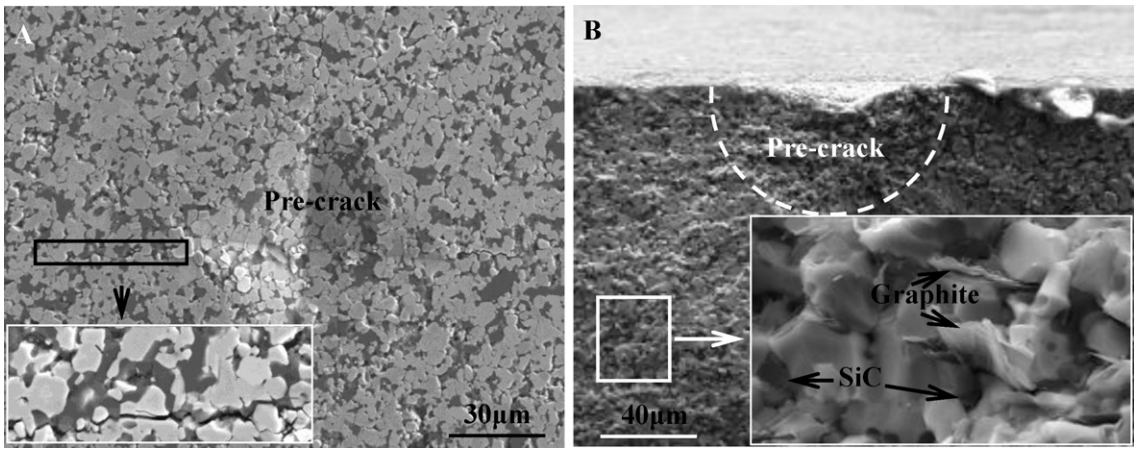

Fig. 1. SEM images of (A) surface shapes and (B) cross-sectional shapes of the crack and indentation.

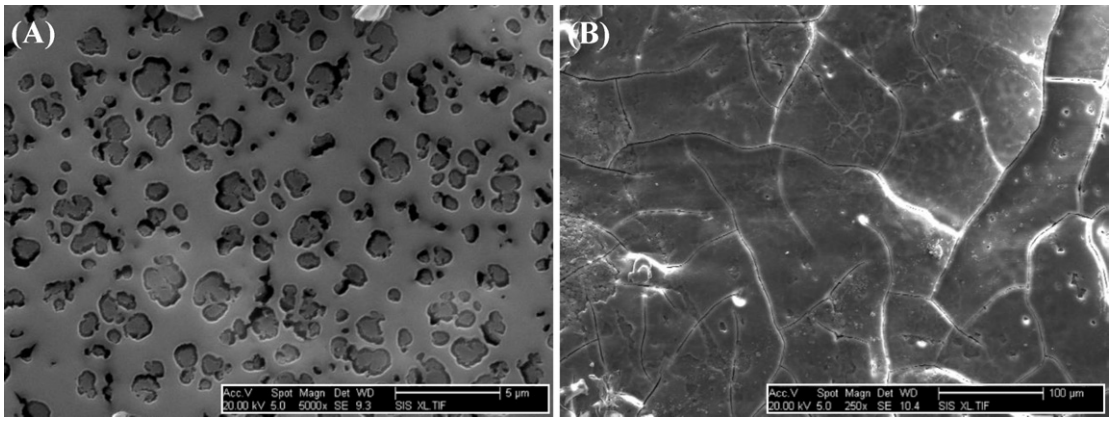

Fig. 2. The micrographs of the surface of the ZrB_2–SiC–graphite ceramic after oxidation at 1100 °C for (a) 30 min and (b) 60 min in dry air.

ZrB_2. The presence of a trace of ZrB_2 was ascribed to thinner oxide layers because of the rapid volatilization of B_2O_3 at 1100 °C [13]. The formation of H_3BO_3 of lamellar structure was due to the extreme sensitivity of B_2O_3 toward hydrolysis in moist air. A negative standard Gibbs free energy of reaction, B_2O_3 would react spontaneously with water in moist air according to Eq. (6), resulting in the formation of H_3BO_3 of layered structure [17]. In summary, the B_2O_3 glass was first formed and then it reacted with water in moist air to the H_3BO_3 of lamellar structure during the specimen was oxidized for 30 min in moist air.

$$\frac{1}{2}B_2O_3(s) + 3H_2O \rightarrow H_3BO_3(s) \quad \Delta_r G_{298} = -28.8 \text{ kJ mol}^{-1} \qquad (6)$$

After oxidation for 30 min in moist air, the specimens exposed to moist air (relative humidity of 35%) at room temperature for 24 h underwent further hydrolysis (Fig. 4). Furthermore, a small quantity of particles with lamellar structures was observed on the surface of the specimen. The borosilicate glass showed better mois-

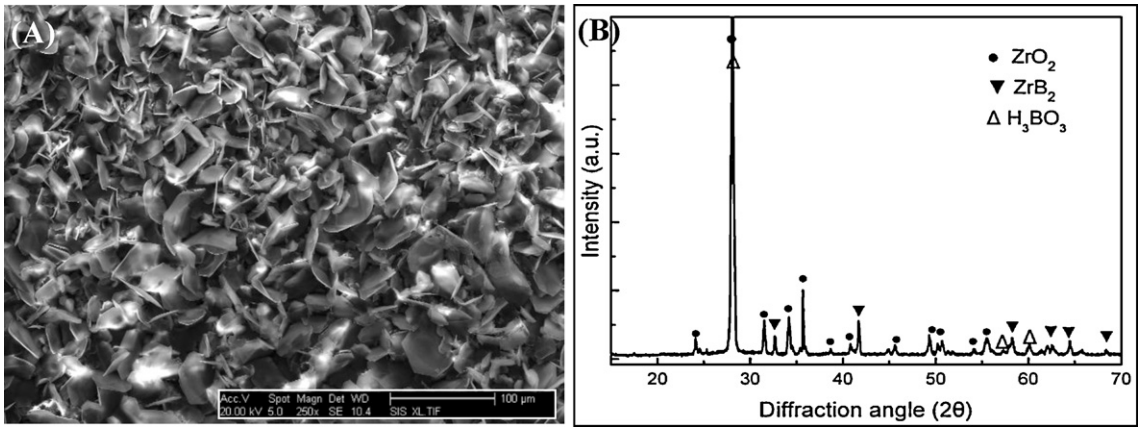

Fig. 3. SEM micrograph (A) of the surface of the specimen oxidized for 30 min in moist air and the typical GXRD spectrum (B) of the specimen oxidation of 60 min in moist air.

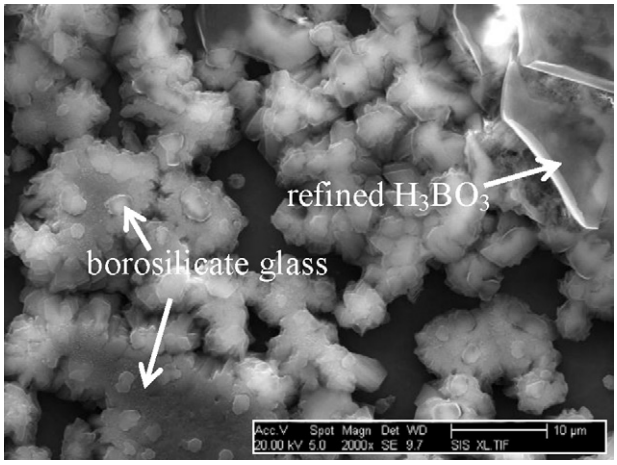

Fig. 4. The micrograph of the surface of the specimen exposed to moist air at room temperatures for 24 h.

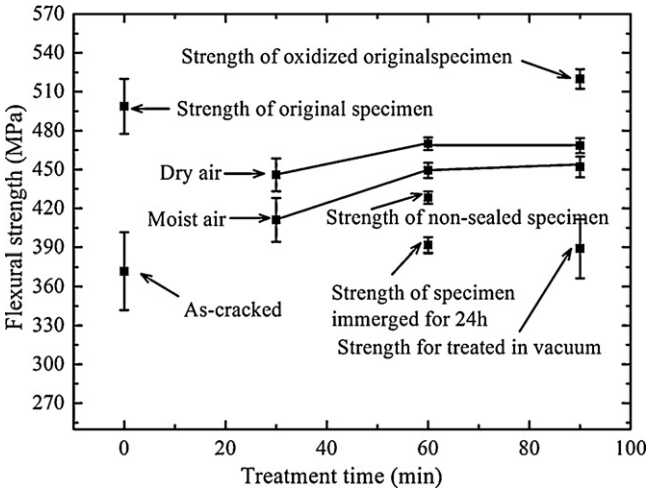

Fig. 6. The flexural strength of the specimen.

ture resistance, lower volatility at high temperature, and higher viscosity than B_2O_3 glass was detected on the surface of the specimen.

To evaluate the hydrolysis resistance of glass structure, the rectangular bars oxidized in moist air for 30 min were immersed in water bath at room temperature for 24 h (Fig. 5). No glassy phase was detected due to the complete hydrolysis of B_2O_3. All the ZrB_2 particles on the surface of the specimen were oxidized to loose ZrO_2 particles and the surface of the specimen was incompletely covered with the loose ZrO_2 particles. Furthermore, a small quantity of borosilicate glass was observed on the loose ZrO_2 particles.

3.2. Flexural strength

Fig. 6 shows the flexural strength of the specimen oxidized in each condition. The flexural strength of the pre-cracked specimen was 371.7 ± 29.9 MPa, which lower than the original strength of 498.8 ± 21.3 MPa. The reduction in flexural strength was ascribed to the presence of the pre-cracks because the ZrB_2–SiC–graphite ceramic is sensitive to the cracks. The flexural strength of the specimens oxidized in dry air increased from 445.9 ± 12.6 MPa to 469.9 ± 4.8 MPa as the treatment time increased from 30 min to 60 min due to the formation of the glass layer. Although cracks below the porous glass layer for the specimen oxidized in dry air for 30 min were found as a result of the oxidation of graphite flake, the strength after oxidation treatment for 30 min was still improved, which was because the sensitivity of a ZrB_2–SiC–graphite ceramic to the cracks was passivated due to oxidation. The flexural strength of the specimens oxidized in moist air for 30 min and 60 min was, respectively, 411.1 ± 16.9 MPa and 449.3 ± 5.8 MPa, which was greater than 371.7 ± 29.9 MPa of the pre-cracked specimen. In spite of dry or moist air healing environments, the flexural strength of the oxidized specimens was recovered as the treatment time up to 60 min and then the flexural strength did not further increase, which revealed that the surface of the specimen was covered with oxide layers in the oxidation of 60 min. The flexural strength of the specimen oxidized in dry air was greater than that of the specimen oxidized in moist air, which revealed that the glassy structure was better able to heal the cracks on the surface of the specimen than the lamellar structure. The lamellar crystals consist of strongly bonded boron, oxygen, and hydrogen atoms. The atomic layers are 0.318 nm apart and held together by van der Waals forces [16]. In a sense, the lamellar crystal structure of H_3BO_3 is similar to the microstructure of the graphite flake, which was detrimental to the healing ability of oxide layers. Compared with 449.3 ± 5.8 MPa for the specimens oxidized in moist air for 60 min, the flexural strength for non-sealed specimens and specimens immersed in water for 24 h was further reduced to 428.2 ± 4.8 MPa and 391.7 ± 9.9 MPa, respectively, due to the hydrolyzation of B_2O_3 glass and the exposure of loose zirconia layer. The further decrease in strength for non-sealed specimens and specimens immersed in water for 24 h also indicated that the dry condition was more favorable than moist air condition

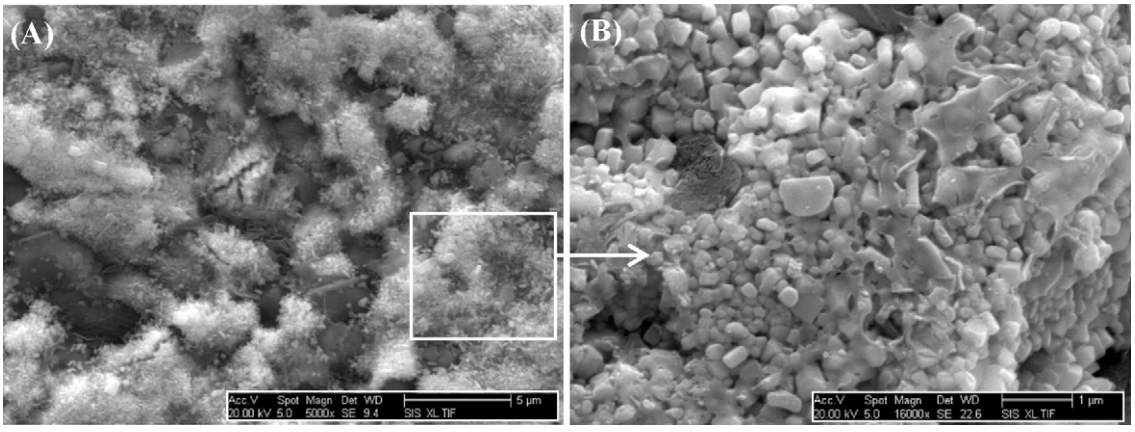

Fig. 5. The micrographs of the surface of the oxidized specimen immersed for 24 h in the waterbath of the room temperature, (A) and (B) were low and high magnification, respectively.

for strength recovery. Compared with 371.7 ± 29.9 MPa of the pre-cracked specimen, the strength of the specimen oxidized in dry and moist air was recovered significantly to 469.9 ± 4.8 MPa and 449.3 ± 5.8 MPa, respectively.

In order to confirm that the increase in strength of the pre-cracked specimen after oxidation treatment was actually an effect of oxide layers, the flexural strength of the pre-cracked specimen treated in vacuum using same conditions for 90 min was greater than that of the pre-cracked specimen, whereas lower than that of the specimen treated in dry and moist airs, as shown in Fig. 6. This indicated that the increase in strength of the pre-cracked specimen after oxidation treatment was actually an effect of oxide layers. Furthermore, the flexural strength of the specimen treated in vacuum was slightly greater than that of the pre-cracked specimen immersed in water for 24 h, which indicated that the heat treatment was favorable to release the residual stress at crack tip. In addition, the original specimen (not pre-cracked) was oxidized in dry air for 90 min and the flexural strength of 519.8 ± 7.6 MPa for the oxidized original specimen was greater than original strength of 498.8 ± 21.3 MPa, which further confirmed that the increase in strength of the pre-cracked specimen after the oxidation treatment was actually an healing effect of glass layer because of the presence of the cracks on the original surface of a ZrB_2–SiC–graphite ceramic [7,18]. Based on above-mentioned results, the increase in flexural strength of the pre-cracked specimen oxidized was mainly attributed to the formation of the oxide layers. Further work on the healing behavior of oxides formed at higher temperature, such as 1200 and 1400 °C is continuing to understand the healing mechanism of the different oxides.

4. Conclusions

Two oxidation conditions were used, dry air and moist air for times of 30, 60, or 90 min. The flexural strength of the pre-cracked specimens was 371 ± 30 MPa, which was lower than the strength of 499 ± 21 MPa of the original specimens. The reduction in flexural strength was ascribed to the presence of the pre-cracks. The flexural strength of the specimens oxidized in dry air increased from 445.9 ± 12.6 MPa to 469.9 ± 4.8 MPa as the treatment time increased from 30 min to 60 min due to the formation of the glass layer. In spite of dry or moist air healing environments, the flexural strength of the oxidized specimens was recovered as the treatment time up to 60 min and then the flexural strength did not further increase, which revealed that the surface of the specimen was covered with oxide layers in the oxidation of 60 min. The flexural strength of the specimen oxidized in dry air was greater than that of the specimen oxidized in moist air, which revealed that the glassy structure was better to heal the cracks on the surface of the specimen than the lamellar structure. Compared with 371.7 ± 29.9 MPa of the pre-cracked specimen, the strength of the specimen oxidized in dry and moist air was recovered significantly to 469.9 ± 4.8 MPa and 449.3 ± 5.8 MPa, respectively.

Acknowledgments

This work was supported by the China Postdoctoral Science Foundation Funded Project (20100481220) and the Fundamental Research Funds for the Central Universities (3014-852001 and DUT10ZDG05) and the National Natural Science Foundation of China (51002019 and 91016024).

References

[1] I. Bogomol, T. Nishimura, Y. Nesterenko, O. Vasylkiv, Y. Sakka, P. Loboda, J. Alloys Compd. (2011), doi:10.1016/j.jallcom.2011.02.176.
[2] I. Bogomol, O. Vasylkiv, Y. Sakka, P. Loboda, J. Alloys Compd. 490 (2010) 557–561.
[3] H.L. Wang, C.A. Wang, X.F. Yao, D.N. Fang, J. Am. Ceram. Soc. 90 (2007) 1992–1997.
[4] C.F. Hu, Y. Sakka, H. Tanaka, T. Nishimura, S. Grasso, J. Alloys Compd. 494 (2010) 266–270.
[5] C.L. Yeh, H.J. Wang, J. Alloys Compd. 509 (2011) 3257–3261.
[6] I. Bogomol, T. Nishimura, O. Vasylkiv, Y. Nesterenko, Y. Sakka, P. Loboda, J. Alloys Compd. 505 (2010) 130–134.
[7] Z. Wang, S. Wang, X.H. Zhang, P. Hu, W.B. Han, C.Q. Hong, J. Alloys Compd. 484 (2009) 390–394.
[8] X.H. Zhang, Z. Wang, X. Sun, W.B. Han, C.Q. Hong, Mater. Lett. 62 (2008) 4360–4362.
[9] S.B. Zhou, Z. Wang, W. Zhang, J. Alloys Compd. 485 (2009) 181–185.
[10] M. Singh, R. Asthana, Mater. Sci. Eng. A 460–461 (2007) 153–162.
[11] C.F. Dong, X.G. Li, Z.Y. Liu, Y.R. Zhang, J. Alloys Compd. 484 (2009) 966–972.
[12] W. Nakao, M. Ono, S.K. Lee, K. Takahashi, K. Ando, J. Eur. Ceram. Soc. 25 (2005) 3649–3655.
[13] W.M. Guo, G.J. Zhang, Y.M. Kan, P.L. Wang, J. Alloys Compd. 471 (2009) 502–506.
[14] A. Rezaie, W.G. Fahrenholtz, G.E. Hilmas, J. Eur. Ceram. Soc. 27 (2007) 2495–2501.
[15] S.J. Gregg, R.F.S. Tyson, Carbon 3 (1965) 39–42.
[16] Z.H. Yang, D.C. Jia, Y. Zhou, Q.C. Meng, P.Y. Shi, C.B. Song, Mater. Chem. Phys. 107 (2008) 476–479.
[17] Z.B. Hu, H.J. Li, Q.G. Fu, H. Xue, G.L. Sun, New Carbon Mater. 22 (2007) 131–134.
[18] X.H. Zhang, L. Xu, S.Y. Du, W.B. Han, J.C. Han, Scripta Mater. 59 (2008) 1222–1225.